Available online at www.sciencedirect.com
ScienceDirect
Engineering Failure Analysis 14 (2007) 978–994
ENGINEERING FAILURE ANALYSIS
www.elsevier.com/locate/engfailanal

Failure analysis of a crude oil pipeline

Cesar R.F. Azevedo *

Department of Metallurgical and Materials Engineering, Escola Politécnica da Universidade de São Paulo, Brazil

Received 9 May 2006; accepted 1 December 2006
Available online 22 January 2007

Abstract

The transversal cracking of a seamed API 5L X46 steel tube belonging to a crude oil pipeline was investigated. The main cracking nucleated in the internal surface of the tube, at the boundary between the heat-affected zone (HAZ) and the weld metal, propagating in a stable mode along the radial and longitudinal directions. Stress raisers, such as welding defects and corrosion pits, were associated to the cracking nucleation. The internal surface of the tube and the cracking surfaces presented a deposit layer, which was rich in Fe, O and S. Diffractometry on the internal identified the presence of a multi-layered corrosion deposit, formed by iron oxide (Fe_2O_3 and Fe_3O_4) and iron sulphides, such as pyrrhotite, mackinawite and pyrite, indicating the action of a H_2S corrosion assisted mechanism. The crack propagation path did not depend on the welding macrostructure, growing perpendicular to both the internal surface and main tensile stresses. Crack propagation was, however, microstructure sensitive, with a more intense branching occurring inside the base metal rather than the HAZ region. Both regions presented cracking (blistering) of the sulphide/matrix interface and microfractographic examination indicated the action of a ductile fracture mechanism linking the H_2 blisters, reinforcing the idea that atomic hydrogen association rather than hydrogen embrittlement was the active mechanism during the cracking of the pipeline. These observations indicated that failure of the pipeline occurred by a stress-oriented hydrogen-induced cracking (SOHIC) mechanism.
© 2007 Elsevier Ltd. All rights reserved.

Keywords: Crude oil pipeline; API 5L X46 steel; Welded tube; Through-thickness cracking; Wet-H_2S corrosion

1. Introduction

Oil and gas distribution via pipeline requires high level of safety and trust aiming at the reduction of costs, increase of operational efficiency and minimisation of accidents. It has been estimated, however, that approximately 40% of the world-wide pipeline network has reached its project life (estimated in 20 years) and efforts have been continually applied to further extend its residual life. The structural integrity evaluation of pipelines is an important tool to minimise the risks of leakage and its impact on the environment,

* Tel.: +55 11 30915691; fax: +55 11 30915243.
E-mail address: c.azevedo@usp.br
URL: www.pmt.usp.br.

1350-6307/$ - see front matter © 2007 Elsevier Ltd. All rights reserved.
doi:10.1016/j.engfailanal.2006.12.001

enhancing the vital importance of the study of defects (cracks and corrosion pits) on the material's integrity. According to the US Environmental Protection Agency, the number of oil spills has been reduced to less than 1% of the total volume handled each year (250 billion gallons of oil and petroleum products), meaning that over 2.5 billion gallons of oil and petroleum are still spilled every year only in the US. Accidents can happen during the oil production, distribution, storage and consumption process and it is very important to possess a detailed contingency plan (containment and recovery actions) to reduce the harmful effects of the oil spill [1–3].

In 1993, for instance, a rupture occurred in an oil pipeline in Virginia (US), sending a 30 m plume of fuel oil into the air. The high-pressure pipeline released over 400,000 gallons of oil to the environment (one of the largest inland oil spills in recent history) before it could be controlled, with the recovery of over 90% of the spilled oil. A number of advanced response mechanisms are available for controlling oil spills and minimising their impacts on human health and the environment. The key to effectively combat oil spills is careful selection and proper use of the equipment and materials best suited to the type of oil and the conditions at the spill site, such as mechanical containment; chemical and biological methods; physical methods (wiping with sorbent materials, pressure washing, and raking and bulldozing); and scare tactics (propane scare-cans, floating dummies, and helium-filled balloons, which are used to protect birds and animals by keeping them away from oil spill areas) [1]. The present paper will investigate the longitudinal cracking of an API 5L X46 steel crude oil pipeline, which caused the inland spill of crude oil that reached a nearby river, causing environmental damages.

2. Experimental procedure and results

The cracking was nucleated on the internal surface of the pipeline, propagating in a stable mode in both radial and longitudinal directions, the latter along the heat affected zone (HAZ) of the seamed steel tube. Non-destructive inspection (magnetic particles) indicated that the through-thickness crack featured a width of 220 mm in the internal surface and 140 mm in the external surface. Visual inspection did not show the presence of a plastically deformed region next to the crack (see Fig. 1a and b). Macrofractographic examination of the exposed surface of the primary crack (see Fig. 1b) revealed the presence of two regions:

- Region 1: plane region (stable crack propagation) with a semi-elliptical format up to a thickness of 7.1 mm, featuring the presence of a dark deposit, which is rich in Fe, O, Si and S (see Table 1);
- Region 2: shear-lip region (approximately 0.5 mm thick), also featuring the presence of a dark Fe-O-Si-S rich deposit (see Table 1), although the contents of O and S are comparatively lower.

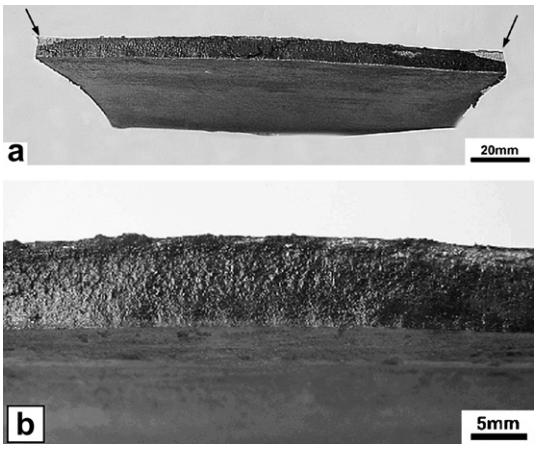

Fig. 1. Visual inspection – longitudinal section, exposed surface of the primary cracking: (a) general view, arrows indicated fresh fracture induced in the laboratory. (b) Detail of the fracture surface showing predominant plane fracture and top edge featuring shear-lip.

Table 1
EDS microanalysis results on the cracking surface

Position	Elements (%)			
	O	Fe	Si	S
Region 1	25	54	8	7
Region 2	9	81	5	2

Macro and microstructural examination of a transversal section of the tube (see Fig. 2a–g) shows the presence of a two-step welding. The welded zone close to the external surface presents a columnar macrostructure, typical of as-cast material, featuring allotriomorphous and Widmanstätten ferrite and colonies of pearlite (see Fig. 2b), indicating that the last welding step was applied on the external surface. The adjacent HAZ region presents a microstructural gradient between two regions:

– Welding/HAZ interface: coarse microstructure composed of colonies of pearlite and allotriomorphous and Widmanstätten ferrite (see Fig. 2c);
– HAZ/metal base interface: refined microstructure composed of ferritic grains and colonies of pearlite (see Fig. 2d).

The welded zone close to the internal surface presents a recrystallised columnar macrostructure composed of ferritic grains and colonies of pearlite (see Fig. 2e), indicating that the first welding step was applied on the this surface. The adjacent HAZ region presents a microstructural gradient between two regions:

– Welding/HAZ interface: recrystallised microstructure composed of colonies of pearlite and elongated ferrite grains (see Fig. 2f);
– HAZ/metal base interface: microstructure composed of ferritic grains and colonies of pearlite (see Fig. 2g).

The microstructure of the tube is aligned along the plate deformation direction, being composed of ferrite grains, colonies of pearlite and sulphide inclusions (some up to 500 μm long), see Fig. 3a and b. The inclusion content of the steel was identified as type A (sulphide) – heavy series – level 2; and type D (globular oxide) – thin series – level 2.

The microstructural results revealed the thermal effect of the second welding step on the recrystallisation of the welded zone of the first welding step, resulting in microstructural refinement and increase on the proportion of ferrite.

The internal surface of the tube presented cracking associated to the presence of welding defects (between 25 and 100 μm deep) and corrosion pits (see Figs. 4a until c and 5c). HAZ regions located in same position along the internal surface of tube presented different microstructures, from ferritic microstructure to pearlitic microstructures with intergranular ferrite (see Figs. 4b and c), indicating that the thermal input during the welding process was not kept constant, causing microstructural asymmetries along the HAZ regions. Fig. 5a and b showed that the direction of crack propagation does not depend on the macrostructure, as the primary crack nucleates on the welding/HAZ interface and grows perpendicular to both the internal surface and the main tensile stresses, propagating along the diverse HAZ and base metal regions.

Microfractographic examination of the exposed surface of the primary crack after careful cleaning of the surface with Clark's solution revealed the presence of:

- a plane surface, until approximately 1.3 mm deep (inside HAZ region), with the presence of numerous parallel secondary cracks (see Fig. 6a and b);
- a rough surface topography inside the base metal region;
- a 45° rough surface (shear-lip) near the external surface of the tube.

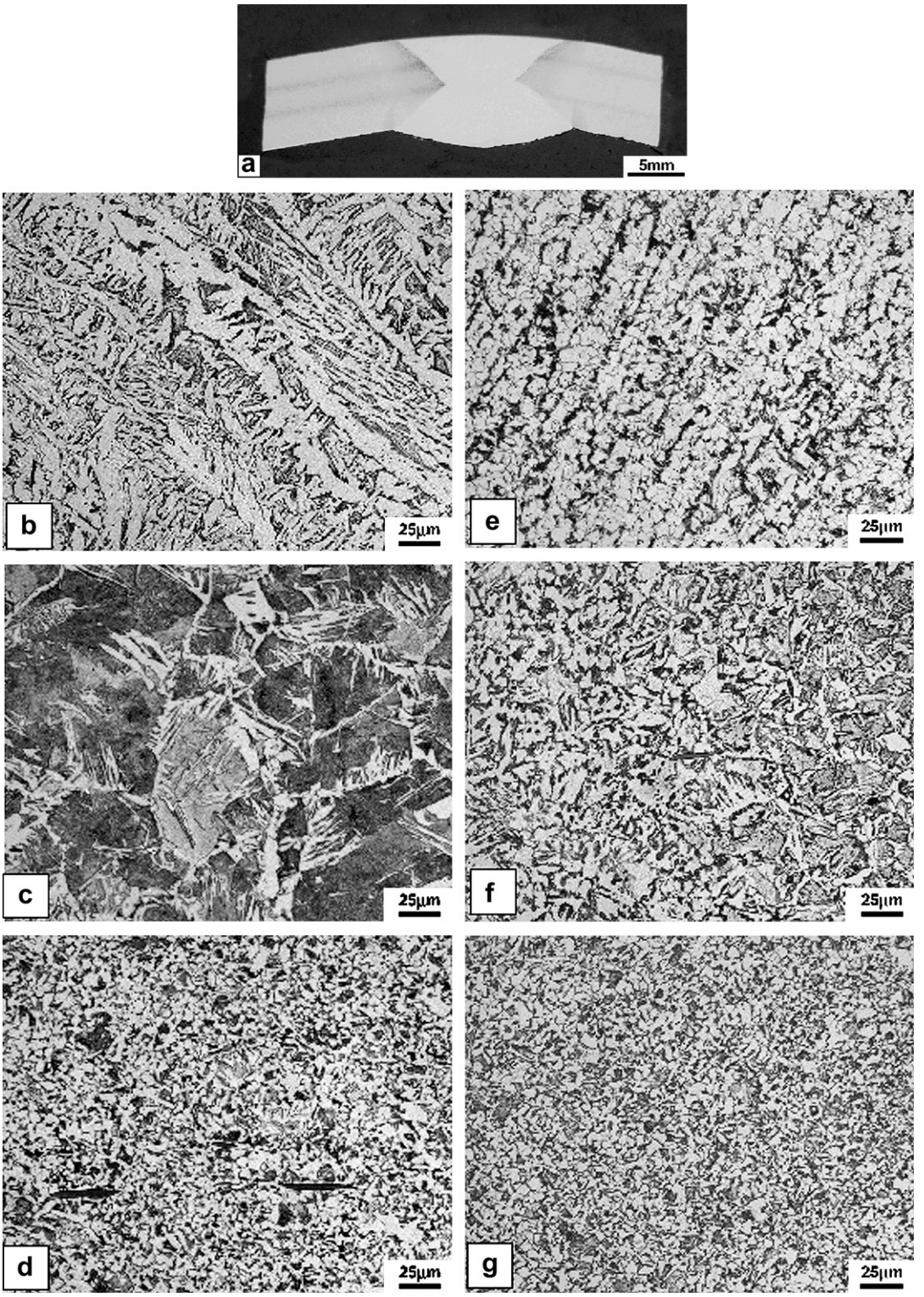

Fig. 2. Microstructural examination – nital etching – welding region – transversal section: (a) general view showing the presence of two-step welding; (b) external surface, welding region, as-cast microstructure; (c) external surface, welding/haz interface; (d) external surface, haz/base metal interface; (e) internal surface, welding region; (f) internal surface, welding/haz interface, recrystallised microstructure; (g) internal surface, haz/base metal interface.

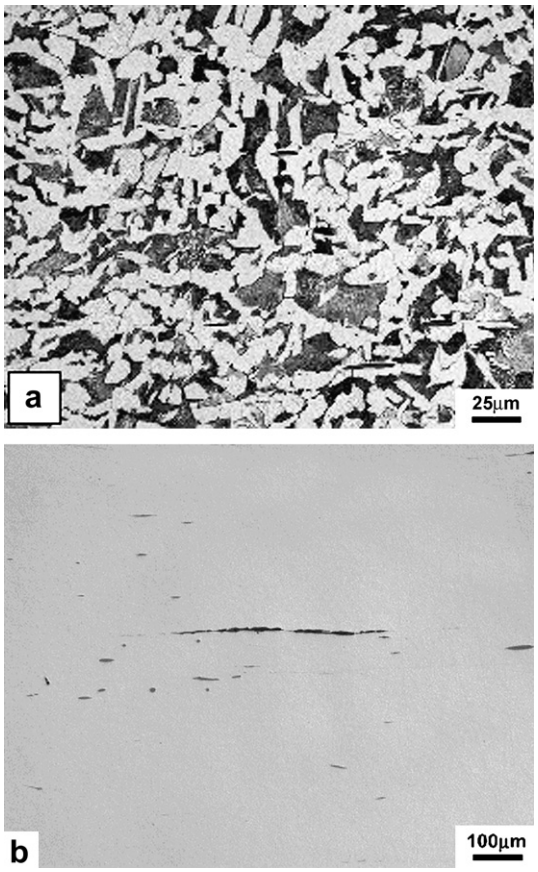

Fig. 3. Microstructural examination – base metal – longitudinal section: (a) ferritic pearlitic microstructure; (b) detail showing sulphide inclusion.

A detailed examination taken between the parallel secondary cracks revealed that both HAZ and base metal regions featured predominately a ductile fracture mode (presence of dimples), see Fig. 6c and d.

Microstructural examination of the primary crack propagation path (see Figs. 7a–9a) revealed that the crack nucleation took place in a superficial heterogeneity (150 μm deep welding defect), which was present at the welding/HAZ interface of the internal surface of the tube (see Fig. 9a), and progressed transgranularly perpendicular to the surface, featuring a moderate intergranular/transgranular branching along the HAZ region (see Fig. 7d). Preferential secondary cracking along the sulphide/matrix interfaces was also observed inside both HAZ and base metal regions (see Figs. 8b and 9b and c), originating the formation of parallel secondary cracks, which were observed during the microfractographic examination (see Figs. 6c, 8b and 9b and c). Within the metal base region, the crack propagation path presented a more intense branching, resulting in the formation of a rougher fracture surface (see Fig. 8c and d). Fig. 9d shows in detail the transgranular nature of the crack propagation inside the HAZ region and the presence of a deposit layer on the crack surface.

EDS microanalysis on the crack deposit layer indicated the presence of Fe, O, Si and S on many positions of the crack propagation (see Table 2), while the diffractometry results (Cu X-ray tube, voltage: 40 kV, current: 40 mA, scan mode: fixed time, sampling pitch: 0.01°, pre-set time: 8 s, scan range ($\Delta 2\theta$): 24–68° conditions) on the deposit layer, which was present on the internal surface of the pipeline near the transversal cracking, revealed the presence of iron oxides (Fe_2O_3 and Fe_3O_4) and many types of iron sulphide (see Table 3 and Fig. 10), such as pyrrhotite, mackinawite and pyrite (multi-layered corrosion deposit). Finally, microhardness mapping (using Vickers hardness measurements – 4.9 N) of the welding region, as requested by ISO 15156-2:(2003) standard, is shown in Fig. 11a and b.

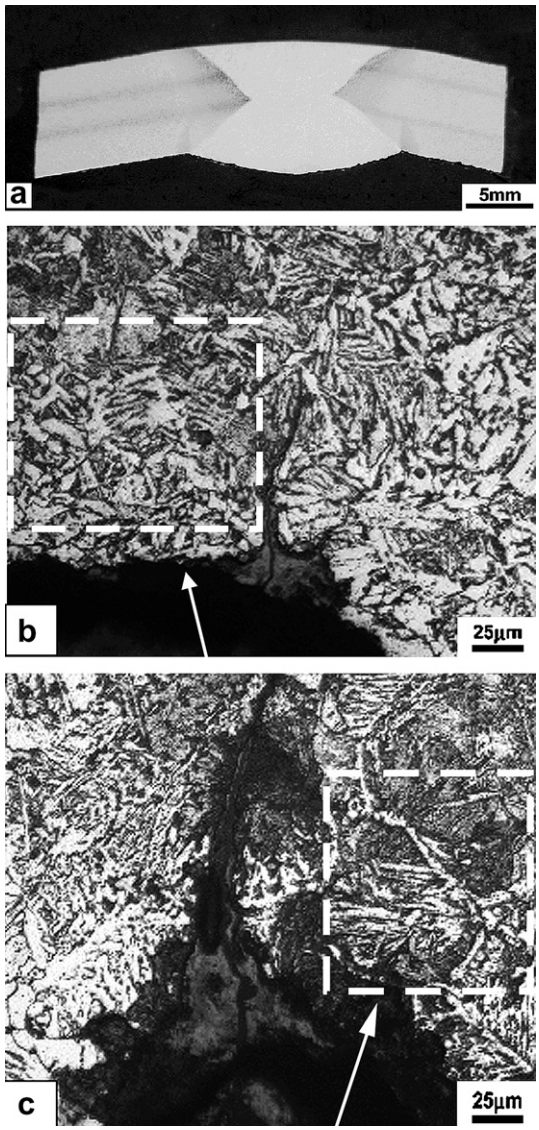

Fig. 4. Microstructural examination – nital etching – welding region – transversal section: (a) general view; (b) and (c) detail of the haz/welding region of the internal surface, left (b) and right position (c), showing transgranular cracking associated to the presence of superficial irregularities (corrosion pits – see arrows). Additionally, symmetrical haz regions present different microstructure (compare dotted areas).

3. Discussion

The formation of a through-thickness cracking occurred by the nucleation and growth of a stable crack (formed on the internal surface of the pipeline, right on the welding/HAZ interface) with a semi-elliptical format up to a thickness of 7.1 mm. After this depth, the crack propagated by an unstable mode, resulting in the formation of a shear-lip region (0.5 mm thick). The nucleation of the primary crack was promoted by the presence of welding defects and corrosion pits, which were found on the internal surface of the tube. Stable crack growth occurred preferentially by transgranular propagation (ductile fracture with formation of dimples) and sulphide/matrix cracking. The internal surface of the pipeline near the crack nucleation site featured, the presence of a multi-layered corrosion film consisting of iron oxides (Fe_2O_3 and Fe_3O_4) and iron sulphides (pyrrhotite, mackinawite and pyrite). These results indicated that the crack propagation occurred by a H_2S corrosion assisted mechanism.

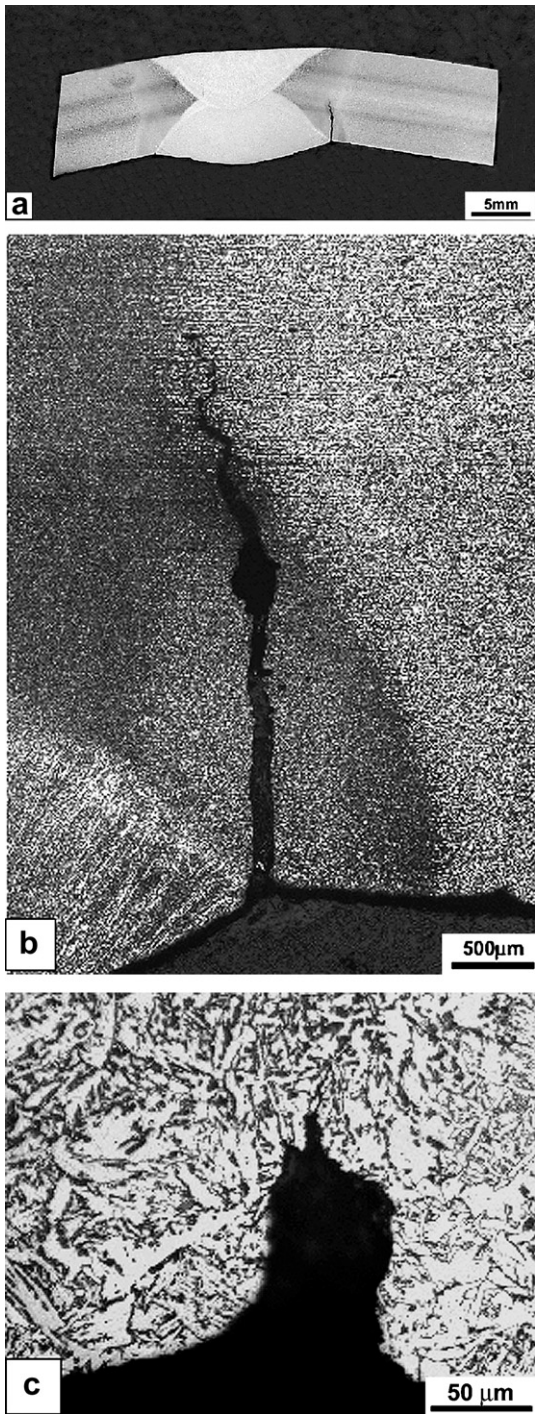

Fig. 5. Microstructural examination – nital etching – welding region – transversal section: (a) general view showing primary cracking; (b) and (c) detail of the haz/welding region of the internal surface, right (b) and left position (c) showing detail of crack propagation path along the haz region (see (b)) and cracking associated to the presence of a welding defect (see (c)).

Crude oil is a heterogeneous mixture of solid, liquid and gaseous phases, which includes sediments, water, salts, acid gases (such as H_2S) and carbon monoxide. Pressure-containing equipment manufactured in carbon-steel and working in environments containing H_2S and water, such as crude oil pipelines, are known to require

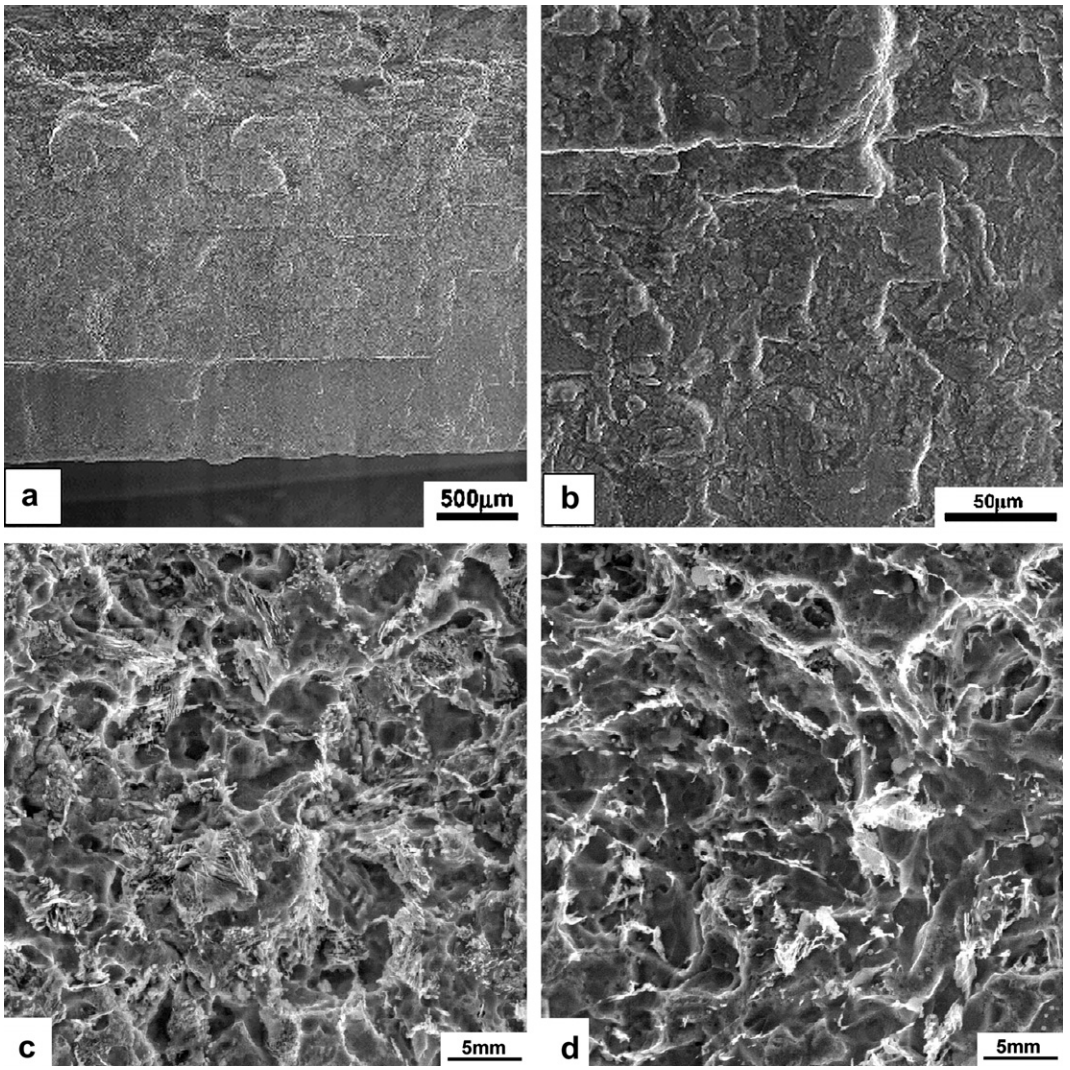

Fig. 6. Microfractographic examination: (a) general view showing plane (bottom and central area) and rough (top area) regions and presence of parallel secondary cracks; (b) detail showing parallel secondary cracks; (c) detail inside the haz (plane surface) region showing predominance of ductile type fracture; (d) detail inside the base metal (rough surface) region showing predominance of ductile type fracture.

special attention in material selection, welding procedures and use conditions in order to avoid the occurrence of H_2S corrosion. In this sense, the concentration of H_2S in the crude oil is one of the process variables, which should be kept under strict control [4–7].

There are many ways to represent the cathodic and anodic reactions during the H_2S corrosion of steel, and two models are described in Table 4. Despite few differences in the description of the reaction steps, the H_2S corrosion of steel generally causes [8–12]:

- the formation of an iron sulphide (Fe_xS_y) film, which sometimes can act as a corrosion barrier;
- the diffusion of atomic hydrogen into the crystal structure of the corroded steel, which may promote its premature failure in service. The presence of H_2S prevents the bubbling of molecular hydrogen, promoting even further the adsorption of atomic hydrogen.

The types of the iron sulphide (Fe_xS_y), which are formed on the surface of the steel during H_2S corrosion, are a key factor controlling the H_2S corrosion and the formation of atomic hydrogen (see Table 5). Their

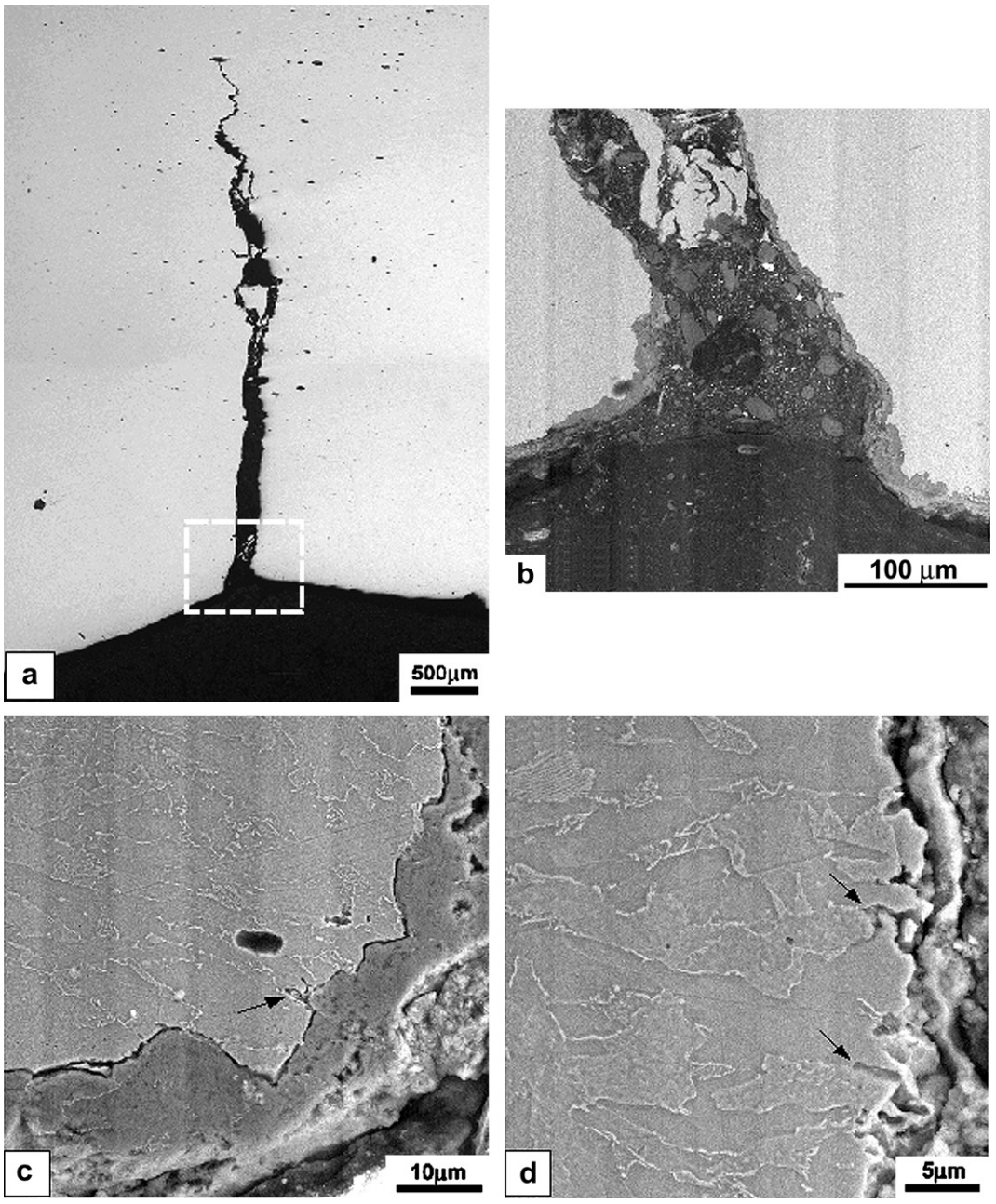

Fig. 7. Microstructural examination – crack propagation path – transversal section – nital etching: (a) general view; (b)–(d) detail near the internal surface (haz region, see dotted area) showing the presence of deposit, rich in Fe, O and S, on the primary crack surface and moderate crack branching (see arrows), SEM-BEI.

formation depends not only on the thermodynamic conditions, such as temperature, pressure and chemical composition of environment and metal, but also on kinetics of sulphide formation, which might lead to the development of metastable iron sulphide phases. The Fe-S binary diagram shows the presence of the following stable iron sulphide phases: α-FeS, β-$FeS_{hP24\text{-hexagonal}}$, γ-$FeS_{hP4\text{-hexagonal}}$ (pyrrhotite), α-$FeS_{2\ oP6\text{-orthorhombic}}$ (marcasite) and β-$FeS_{2\ cP12\text{-cubic}}$ (pyrite). Metastable disordered mackinawite is a highly reactive phase with a high adsorptive capacity for divalent metals, and it is usually the first iron sulphide to form in most ambient

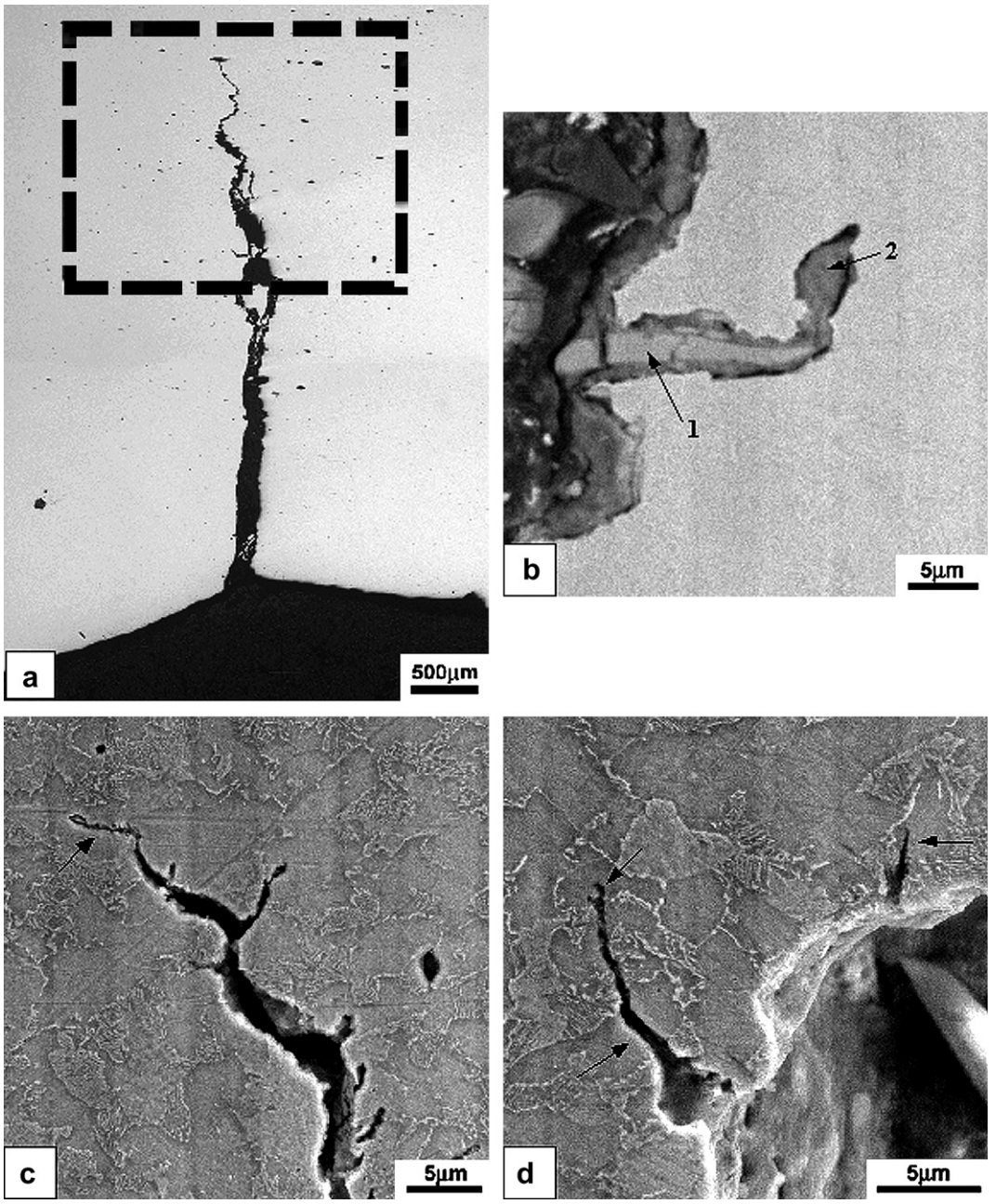

Fig. 8. Microstructural examination – crack propagation path – transversal section – nital etching: (a) general view; (b)–(d) detail inside the base metal region (see dotted area) showing more intense crack-branching (see arrows) and sulphide/matrix delamination associated with the presence of deposit layer, rich in Fe, O and S, on the crack surface (see arrows 1 and 2), SEM-BEI.

environments. With time, it reacts to form more stable iron sulphide phases, such as metastable ordered mackinawite, metastable greigite, and ultimately stable pyrite or pyrrhotite. Pyrite and pyrrhotite films feature a more protective barrier against corrosion, while mackinawite, found during the experimental work (see Table 3 and Fig. 10), is the less protective iron sulphide film [8–10].

The presence of atomic hydrogen produced by H_2S corrosion can cause deleterious effects on the microstructure and mechanical properties of steels, as it diffuses into its crystal structure and interacts with defects,

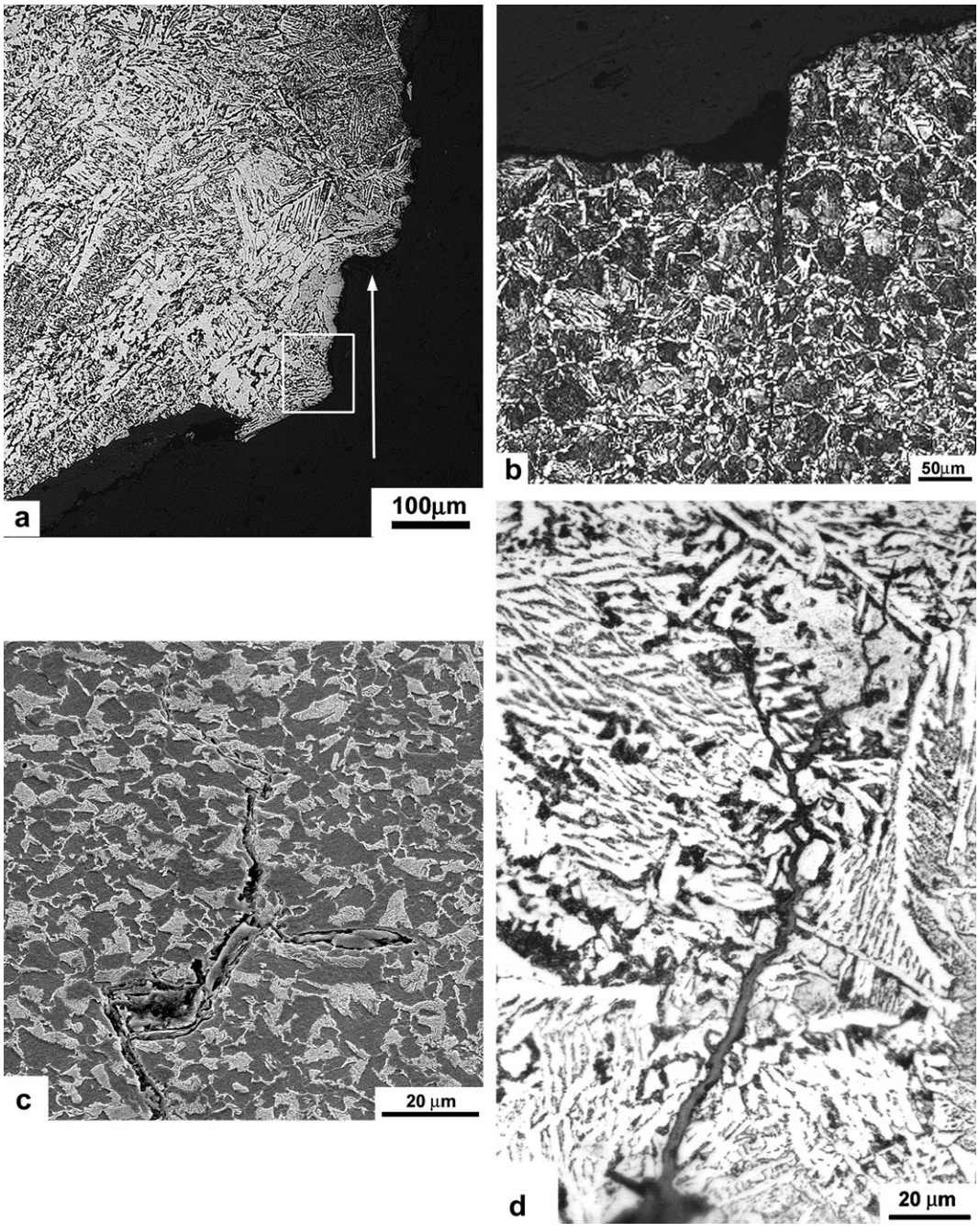

Fig. 9. Microstructural examination – crack propagation path – transversal section located in the middle of the elliptical fracture surface-nital etching: (a) presence of a 150 μm deep welding defect associated with the nucleation of the primary cracking, see arrow; (b) sulphide/matrix delamination inside the haz region; (c) sulphide/matrix delamination inside the base metal; (d) transversal cracking inside the haz region and presence of a deposit layer on the crack surface.

such as dislocations and inclusions. Besides the microstructural embrittlement by atomic hydrogen, the association of atomic hydrogen species inside the iron crystal may lead to the formation of H_2 on special sites, which may cause the deformation of the surrounding metallic matrix or even, under more critical circumstances, its cracking (blistering) due to the high pressure of gaseous hydrogen given by the equilibrium $2\underline{H} \rightarrow H_2$ (g) [8–13].

Table 2
EDS microanalysis results on the deposit layer found on the primary and secondary cracking (balance is Fe)

Position	Elements (%)	
	O	S
Deposit layer on the primary cracking (Fig. 7c)	39	7
Deposit layer on the tip of the primary cracking (Fig. 8c)	45	5
Deposit layer on matrix/sulphide interface (Fig. 8b)	42	4

Table 3
Diffractometry results on the internal surface of the pipeline near the transversal cracking

Peak number	Interplanar spacing $\langle d \rangle$ (Å)	$\langle I_r \rangle$ Relative intensity	Possible phases[a]
11	2.0262	100	Ferrite (110) Pyrrhotite (102)
5	2.53707	24	Fe_3O_4 (311) Fe_2O_3 (110)
19	1.48437	22	Fe_3O_4 (440) Fe_2O_3 (214)
1	2.96528	20	Fe_3O_4 (220) Pyrrhotite (100) Mackinawite (101)
20	1.43363	20	Ferrite (200)
3	2.7098	19	Fe_2O_3 (104) Pyrite (200)
17	1.61576	16	Fe_3O_4 (511)
14	1.73618	14	Mackinawite (201)
10	2.09768	13	Fe_3O_4 (400)
2	2.79284	10	Pyrite (200)
13	1.83858	10	Fe_2O_3 (024) Mackinawite (200)
16	1.63393	10	Fe_3O_4 (511) Pyrite (311)
4	2.63175	9	Pyrrhotite (101)
6	2.42283	9	Fe_3O_4 (210) Pyrite (222)
9	2.14959	9	Fe_2O_3 (113)
12	1.91758	8	Pyrite (220)
15	1.72054	8	Pyrrhotite (110) Mackinawite (201)
7	2.30226	5	Fe_2O_3 (006) Mackinawite (111)
8	2.21165	5	Fe_2O_3 (113) Pyrite (211)
18	1.51525	4	Mackinawite (103)

[a] Source: pyrite: JCPSD no. 42-1342; pyrrhotite: JCPSD no. 75-0602; mackinawite: JCPSD no. 15-0039; Fe_3O_4: JCPSD no. 88-0868; Fe_2O_3: JCPSD no. 87-1169; and ferrite: JCPSD no. 06-0698.

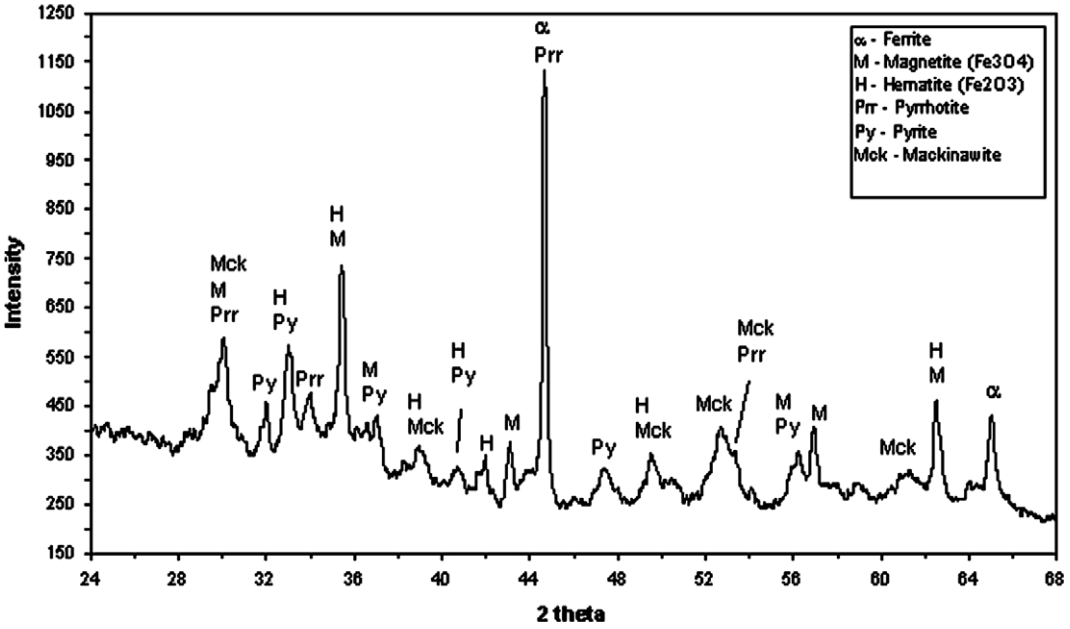

Fig. 10. Diffractometry results (Cu X-ray tube, voltage: 40 kV, current: 40 mA, scan mode: fixed time, sampling pitch: 0.01°, pre-set time: 8 s, scan range ($\Delta 2\theta$): 24–68°) on the deposit layer, which was present on the internal surface of the pipeline near the transversal cracking.

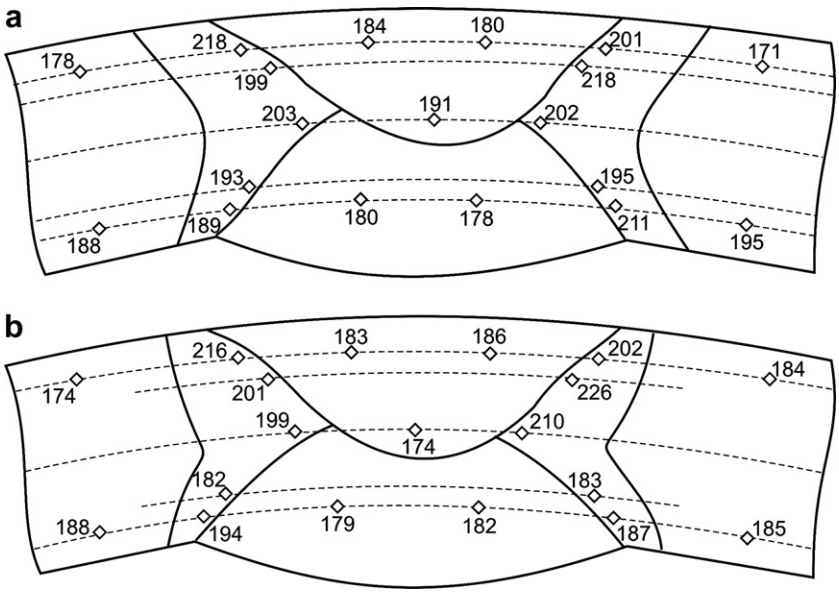

Fig. 11. Hardness mapping across two regions of the welding-transversal section.

Sulphide-stress cracking, for instance, is defined as the cracking under the combined action of tensile stress and corrosion in the presence of water and hydrogen sulphide (a form of hydrogen-induced stress corrosion cracking), causing the hydrogen embrittlement of the metal [14–18]. In 1975 the National Association of Corrosion Engineers published the first edition of a standard concerned with the consequences of sudden failures of metallic compounds used in the oil and gas field and associated with their exposure to H_2S-containing fluids. This standard established limits of H_2S-partial pressure above which precautions against sulphide stress cracking were always considered necessary [14].

Table 4
Cathodic and anodic reactions during H_2S corrosion of steel

Model I	
Cathodic reactions:	$H_2S + e^- \rightarrow HS^- + H^0$ $H_2S + H^0 + e^- \rightarrow HS^- + H_2$ (g) --- $H_2S + 2e^- \rightarrow 2HS^- + H_2$ (g)
Anodic reactions:	$Fe + HS^- \rightarrow (FeHS^-)_{ads}$ $(FeHS^-)_{ads} \rightarrow FeHS^+ + 2e^-$ --- $FeHS^+ \rightarrow Fe^{2+} + HS^-$
Model II	
Cathodic reactions:	$H_2S \rightarrow HS^- + H^+$ $HS^- + e^- \rightarrow H^0 + S^{-2}$
Anodic reaction:	$Fe^+ \rightarrow Fe^{2+} + 2e^-$
General reaction	$Fe^{2+} + HS^- \rightarrow Fe_xS_y + H^+$
Hydrogen dissociation	H_2 (g) $\rightarrow 2\ H^0$
Atomic hydrogen adsorption and association	$2\ H^0 \rightarrow 2\underline{H}$ $2\underline{H} \rightarrow H_2$ (g)

Table 5
Types of iron sulphides

Formulae		Name	Crystal structure	Features
$FeS_{(1-x)}$	$x = 0.0057$–0.064	Mackinawite	Tetragonal	Metastable Black Non-stoichiometric Non-protective film S deficient (type-p semiconductor)
FeS	–	Troilite	Hexagonal	Stable Black Stoichiometric
$Fe_{(1-x)}S$	$x = 0$ to 0.14	Pyrrhotite	Monoclinic Hexagonal	Protective film Non-stoichiometric Brown Fe deficient (type-n semiconductor)
Fe_3S_4	–	Greigite	Cubic	Metastable Brown
$Fe_{(3+x)}S_4$	$x = 0$ to 0.25	Smythite	Hexagonal	metastable Brown
FeS_2	–	Marcasite	Orthorhombic	Yellow S deficient
FeS_2	–	Pyrite	Cubic	Protective film Yellow S deficient or Fe deficient

According to DIN EN ISO 15156-2:2003 standard [15], however, the investigated API 5L X46 steel is not susceptible to sulphide-stress cracking under the pipeline working conditions (pH > 3,5 and H_2S partial pressure > 0.3 kPa). Additionally, EN ISO 15156-1 standard [14] states that the hardness of welds, heat-affected zones and base metal of the pipeline play an important role in determining its sulphide stress cracking susceptibility, which is high in regions presenting hardness greater than 22 HRC or 249 HV (see Table 6). The results of hardness mapping (see Fig. 11a and b) confirmed that the investigated pipeline is not susceptible to sulphide-stress cracking mechanism.

Table 6
Summary of the effects of hardness and stress on hydrogen cracking by H_2S

Type of damage	Wrought steel		Weld metal		Heat-affected zone	
	Hardness	Stress	Hardness	Stress	Hardness	Stress
Blistering	Occurs <249 HV	No	Not susceptible		Occurs <249 HV	No
HIC	Occurs <249 HV	No	Not susceptible		Occurs <249 HV	No
SOHIC	Occurs <249 HV	Yes	Not susceptible		Occurs <249 HV	Yes
SSC	Occurs >249 HV	Yes	Occurs >249 HV	Yes	Occurs >249 HV	Yes

Other types of damage caused by H_2S are more related to the association reaction of atomic hydrogen that takes place within the iron crystal than to the hydrogen embrittlement mechanism. Hydrogen blistering, for instance, is the formation of macroscopic subsurface planar cavities, due to the action of the hydrogen association reaction ($2\underline{H} \rightarrow H_2$), which leads to the formation of excessive internal hydrogen pressure at the internal sites, such as large non-metallic inclusions, causing interfacial decohesion and the formation of H_2 blisters, which might produce internal parallel secondary cracks, as observed during the present investigation. Hydrogen-induced cracking (HIC) is the stepwise internal cracking caused by the formation of hydrogen blisters, connecting adjacent hydrogen blisters on different planes in the metal. It is commonly found in steels with high impurity levels, leading to a high density of planar inclusions and/or regions of anomalous microstructure produced by segregation. An interesting feature of these two mechanisms is that no external applied stresses are needed for their formation [8–10,19,20], contrary to the working conditions of the investigated pipeline.

Finally, stress-oriented hydrogen-induced cracking (SOHIC) occurs under the influence of applied or residual stress and produces arrays of cracks in steel, aligned nearly perpendicular to the applied stress, that are formed by the link-up of small HIC cracks in the steel. It can be, therefore, understood as a two step mechanism, where the former step is the process of hydrogen induced blister cracking (blister cracks parallel to applied stress), and, in the latter stage, the blister cracks link together perpendicularly to the applied stress. The balance between the applied stress and environmental corrosivity should define the final fracture topography in terms of the proportion between brittle and ductile fractures [8–10,21,22]. According to Crag [13], it is unfortunate that very often when investigators observe a new morphology of cracking by H_2S corrosion, they establish a new name for the cracking mechanism regardless whether this is justified mechanistically. Furthermore, the various types of damage caused by H_2S are often associated, as the conditions contributing to one type of damage can contribute to the occurrence of other types of damage, so its not surprising to find a combination of these mechanisms in action.

The investigated pipeline presented a maximum primary stress (σ_1) of approximately 80% of the yield stress of the API 5LX46 steel, considering the presence of stress raisers. Additionally, the experimental results indicated that direction of the crack propagation did not depend on the welding macrostructure and that the main cracking propagated indeed perpendicular to both the internal surface and the main tensile stresses. The crack propagation path was, however, microstructure sensitive, with a more intense branching occurring inside the base metal rather than the HAZ region. Furthermore, both regions presented preferential cracking (blistering) of the sulphide/matrix interface and possible formation of a multi-layered corrosion film on the surfaces of primary and secondary cracks. Finally, the microfractographic examination suggested the action of a ductile fracture mechanism linking the H_2 blisters, reinforcing the idea that atomic hydrogen association rather than hydrogen embrittlement was the active mechanism during the cracking of the pipeline. These results indicated the predominant action of a stress-oriented hydrogen-induced cracking mechanism. DIN EN ISO 15156-2:2003 standard [15] states indeed that the user should consider the possible action of SOHIC mechanism when evaluating carbon steel plates forms and their welded products subjected to sour service in H_2S-containing environments.

According to previous research [22], the methodology for preventing HIC (where no stress is needed) is also effective for the prevention of SOHIC. In this sense, accelerated cooling over conventional normalising was reported to be effective, since SOHIC propagation is microstructure sensitive and regions with minimum microhardness were observed to become a preferential site for crack nucleation. Additionally, soft regions also provide plastic zones through which the existing blisters are prone to link to each other, leading to the crack

growth through the thickness. As a consequence, the local decrease in hardness observed in some regions of the HAZ, which were caused by the heating effect of the second welding step on the first welding step, may have enhanced the SOHIC susceptibility of the investigated pipeline.

Non-metallic inclusions were also identified as preferential crack nucleation sites and the investigators calculated a critical dispersion distance of inclusions, within which a second blister can be induced in the plastic zone formed around the first blister, indicating that the dispersion of non-metallic inclusions is an important variable to avoid SOHIC [22]. In this sense, it's recommended the use of steel with a lower inclusion content than the one observed experimentally for the investigated API 5LX46 steel pipeline in order to decrease its SOHIC susceptibility.

The effect of the microstructure on the SOHIC resistance was also investigated by Cayard and Cooke [21] through a comparative study between conventional and HIC resistant steels. Samples were welded, mounted under stress (90% of the yield strength) and placed in an aqueous solution of NaCl, glacial acetic acid and saturated with H_2S gas (pH 3.3). Both microstructures showed the presence of ferrite and pearlite, but the conventional steel showed microstructural banding, with higher proportion of elongated sulphides and higher volumetric fraction of pearlite. The cracking of the HIC resistant steel (without microstructural banding) occurred on a nearly straight path, while the conventional material (with microstructural banding) presented a jagged propagation path, with discrete steps, equivalent to the pearlite band spacing. The present investigation confirmed that the base metal region, with a banded microstructure, featured a jagged crack propagation path, while the recrystallised HAZ region, with a more equiaxial microstructure, feature a straight crack propagation.

The investigators [21] also showed that the fracture surface morphology of the conventional steel was highly woody, with the presence of quasi-cleavage with some traces of microvoid coalescence due to the combination of heavily banded microstructure and cracking along sulphide inclusions, while in the HIC resistant steel the fracture surface morphology was highly flat due to the cleavage of the ferritic regions [21]. The present investigation, however, showed a more ductile fracture (microvoid coalescence) aspect, confirming that the final SOHIC fracture topography is defined by the balance between the applied stress, environmental corrosivity and microstructure.

Finally, we recommend that a large extension of the pipeline located near the pumping station, where the H_2S concentration is higher, should be thoroughly examined for the presence of H_2S cracking. All segments of the pipeline subjected to H_2S corrosion should be replaced by a more SOHIC resistant steel and the concentration of H_2S in the crude oil should be kept under strict control.

4. Conclusions

- The formation of a through-thickness cracking occurred in the internal surface of the pipeline by the nucleation and growth of a stable crack formed on the welding/HAZ interface;
- The nucleation of the primary crack was associated to the presence of welding defects and corrosion pits;
- Stable crack growth occurred preferentially by transgranular ductile propagation, with additional presence of sulphide/matrix cracking;
- The cracks featured a multi-layered corrosion deposit, consisting of iron oxides (Fe_2O_3 and Fe_3O_4) and iron sulphides, such as pyrrhotite, mackinawite and pyrite, indicating the action of a H_2S corrosion assisted mechanism;
- Microhardness mapping confirmed that the investigated pipeline is not susceptible to sulphide-stress cracking;
- The crack propagation path did not depend on the welding macrostructure, propagating perpendicular to both internal surface and main tensile stresses;
- Crack propagation was microstructure sensitive, with a more intense branching occurring inside the base metal rather than the HAZ region. Both regions presented preferential cracking of the sulphide/matrix interfaces;
- Microfractographic examination indicated the occurrence of a ductile fracture mode linking the H_2 blisters, which were observed along the sulphide inclusions, reinforcing the idea that atomic hydrogen association rather than hydrogen embrittlement was the active mechanism during the cracking of the pipeline;
- The failure of the pipeline occurred by a stress-oriented hydrogen-induced cracking (SOHIC) mechanism.

References

[1] U.S. Environmental Protection Agency. http://www.epa.gov.

[2] Papadakis GA. Major hazard pipelines: a comparative study of onshore transmission accidents. J Loss Prevent Process Ind 1999;12:91–107.

[3] Personal communication. Prof. Dr. Cláudio Ruggieri.

[4] Cayard MS, Kane RD, Joia CJB, Correa LA. Hydrogen flux monitoring devices in wet H_2S service. PTQ SUMMER; 1999. p. 71–7. http://www.eptq.com/Pages/Articles/Summer1999.htm.

[5] Bruno TV, Craig BD, McHaney JH. Welding structure for sour service. http://www.metallurgical.com/Publications/Publication%2020.pdf).

[6] Cassarini G. Problems related to safety and reliability of materials in environments polluted by hydrogen sulphide. Inst J Press Vess Piping 1993;55:313–22.

[7] Donham JE. Corrosion in petroleum production operations. Metals handbook, vol. 13. Corrosion. 9th Ed. ASM International; 1987. p. 1232–61.

[8] Silva PR. Estudo de aplicação de técnica eletroquímica para monitoramento da corrosão em unidades de craqueamento catalítico fluido. MEng thesis. Universidade Federal do Paraná; 2002.

[9] Esteves FC. Alguns resultados sobre a corrosão pelo H_2S: medidas de impedância e permeação ao hidrogênio. M. Sc. Thesis. 1997. Universidade Federal do Rio de Janeiro.

[10] Alves LFC. Efeito de pequenas adições de H_2S na corrosão pelo CO_2: Estudo efetuado com um novo sistema de ensaios eletroquímicos sob condições controladas de fluxo e pressão. MSc thesis. 1997. Universidade Federal do Rio de Janeiro.

[11] Tseung CC, Sriskandarajah T, Chan HC. A method for the inhibition of sulphide stress corrosion cracking in steel – I. Electrochemical aspects. Corrosion Sci 1985;25(6):383–93.

[12] Carneiro RA, Ratnapulie RC, Lins VFC. The influence of chemical composition and microstructure of API pipeline steels on hydrogen induced cracking and sulfide stress corrosion cracking. Mater Sci Eng A 2003;357:104–10.

[13] Hydrogen damage. In: B. Craig. ASM Handbook, vol. 13A. Corrosion: fundamentals, testing, and protection. 10th ed. ASM International; 2003.

[14] EN ISO 15156-1:2001 international standard. Petroleum and natural gas industries – materials for use in H_2S-containing environments in oil and gas production. Part1: General principles for selection of cracking-resistant materials.

[15] DIN EN ISO 15156-2:2003 standard (Erdöl-, petrochemische und Erdgasindustrie – Werkstoff für den Einsatz in H_2S-haltinger Umbebung bei der Öl-und Gasgewinnun – Teil 2: Gegen Rissbildung beständige unlegiete und nidriglegierte Stähle und die Verwendung vom Gusseises).

[16] Rsay LW, Chen YC, Chan SLI. Sulfide stress corrosion cracking and fatigue crack growth of welded TMCP API 5L X65 pipe-line steel. Int J Fatigue 2001:101–13.

[17] Erlings JG, de Groot HW, Nauta J. The effect of slow plastic and elastic straining on sulphide stress cracking and hydrogen embrittlement of 3.5% Ni steel and API 5L X60 pipeline steel. Corrosion Sci 1987;27(10/11):1153–67.

[18] Kawashima A, Hashimoto K, Shimodaira S. Hydrogen electrode reaction and hydrogen embrittlement of mild steel in hydrogen sulphide solution. 1976;32(8):321–31.

[19] Domizzi G, Anterie G, Ovejero-García J. Influence of sulphur content and inclusion distribution on the hydrogen induced blister cracking in pressure vessel and pipeline steels. Corrosion Science 2001;43:325–39.

[20] Hyodo T, Iino M, Ikeda A, Kimura M, Shimizu M. The hydrogen permeation and hydrogen-induced cracking behaviour of pipeline in dynamic full scale tests. Corrosion Sci 1987;27(10/11):1077–98.

[21] Cayard MS, Cooke DL. An exploratory examination of the effect of SOHIC damage on the fracture resistance of carbon steels. http://www.corrosionsource.com/CS2000/session11/paper1101/paper1101.htm.

[22] Takahashi A, Ogawa H. Influence of microhardness and inclusion on stress oriented hydrogen induced cracking of line pipe steels. ISIJ International 1996;36(3):334–40.